

A CFD Assessment of Film Coating Process Viscosity Models

Sergio Alonso[†], François Bertrand and Philippe A. Tanguy*

URPEI, Department of Chemical Engineering, École Polytechnique, P.O. Box 6079, Station Centre-Ville, Montréal, QC H3C 3A7, Canada

The film coating technique is used for the surface treatment of fragile webs, as very little stress is applied to the substrate, contrary to blade coating. Film coating is also known to produce a contour-like coating with superior coverage even at high process speeds (Wickström and Grön, 2000). These advantages are achieved due to the use of a pre-metering step, in which a thin coating film is first formed in a metering section, before being applied to the substrate. In the metering nip, the film is formed between a small smooth metering rod and a large-diameter soft transfer roll. The metered film characteristics depend on the coating formulation and the nip flow conditions, which are in turn governed mainly by the load exerted on the roll by the rod, the speed, and the roll cover hardness. Since the metered film is an essential part of the final product, a thorough understanding of the metering nip flow is central to the better design of film coating equipment.

In coating processes, thin films of the order of a few tens of microns are produced. In order to obtain such thin coatings and to avoid roll damage, a deformable cover on the transfer roll is essential. The use of an elastic cover results in a fluid–solid boundary that changes according to the hydrodynamics of the flow. In practice, the fluid domain, which is influenced by the equilibrium between flow and elastic forces, is difficult to describe. Coyle (1988) used the lubrication theory to model such fluid domain and described the deformation of the roll cover as simple Hookean springs. He reported that the maximum pressure is lower than that with rigid rolls. In terms of coating thickness, he identified two load regions of different slopes, similar to those observed experimentally at high speeds with Newtonian fluids and suspensions (Réglat and Tanguy, 1997, 1998; Alonso et al., 2000). Carvalho and Scriven (1993) compared three methods to describe the deformation of the elastic cover. Since the one proposed by Coyle (1988) gave results similar to those of the other models, Carvalho and Scriven (1993) concluded that the spring model was reliable enough for practical design considerations. The lubrication theory, however, does not account for the effect of the hydrodynamic stresses on the deformation, and the spring model does not allow for sideways displacements or incompressible covers.

Fourcade et al. (1999) proposed a novel model for the deformation of a Hookean incompressible cover that allows for sideways displacements generated by fluid stresses. For Newtonian fluids, the calculated maximum pressure was compared to that measured experimentally. The results showed similar trends although quantitative differences were

Computer fluid dynamic simulations of the metering nip flow were used to assess the process viscosity of the coating colours. The numerical solution was based on a Galerkin/finite element technique that included the deformation of the roll cover to better represent the flow elastohydrodynamics. The Navier-Stokes prediction was compared with experimental measurements of torque and pressure in the metering nip. From the comparisons, the process viscosity determined in a region of shear-dominated flow is the one, among the three models analyzed, that can better describe the hydrodynamics of the metering nip flow. To improve further the fluid flow numerical description, this process viscosity was combined with an adapted transient Cross model. This new semi-analytical rheological model decreased the differences between the numerical and experimental results. The findings also suggested that the model requires further enhancements, topic that will be addressed in future work.

On a utilisé la simulation par ordinateur des écoulements dans une pince de dosage pour déterminer la viscosité de procédé des sauces de couchage. La solution numérique basée sur la méthode des éléments finis de Galerkin tient compte de la déformation de l'enveloppe du rouleau afin de mieux représenter le comportement élastohydrodynamique de l'écoulement. La prédiction a été comparée à des mesures expérimentales du couple et de la pression dans la pince de dosage. On a pu montrer que la viscosité de procédé déterminée dans la région de l'écoulement dominée par le cisaillement est celle qui, des trois modèles analysés, peut le mieux décrire l'hydrodynamique de l'écoulement dans la pince de dosage. Afin d'améliorer encore la description numérique de l'écoulement du fluide, cette viscosité de procédé est combinée à un modèle de Cross adapté au cas instationnaire. Ce nouveau modèle rhéologique semi-analytique permet de réduire l'écart entre les résultats numériques et expérimentaux. Les résultats suggèrent également que le modèle nécessite d'autres améliorations, un thème qui sera étudié dans des travaux ultérieurs.

Keywords: process viscosity, metering nip, maximum pressure, torque, coating colour.

*Author to whom correspondence may be addressed. E-mail address: tanguy@urpei.polymtl.ca

[†] Present address: CIATEC, A.C., Omega 201, Fracc. Ind. Delta, León, Gto., México 37540.

observed. They were attributed to the uncertainty associated with the measurement of the metering rod position relative to the transfer roll (apparent nip gap), and three-dimensional and free surface effects (Fourcade et al., 1999).

An improvement in the coating flow simulations was achieved by including the free surface downstream from the nip. Carvalho and Scriven (1997), using the lubrication theory, adapted a viscocapillary model for the free surface to a spring-like model for the roll deformation. They found that the deformation of the cover reduces the pressure and delays the onset of the ribbing pattern to higher capillary numbers. Carvalho and Scriven (1999) improved the numerical treatment of the forward roll coating problem by carrying out a three-dimensional flow stability analysis, together with a spring-like model for the roll deformation. Their results confirmed that the deformable cover decreases the pressure gradients and delays the onset of instabilities.

In reverse roll coating flows, the numerical treatment of the free surface is very complex. The three-phase dynamic wetting line leads to a non-integrable stress singularity, so that a slip hypothesis must be implemented (Coyle et al., 1990; Hao and Haber, 1999). The dynamic contact angle needs to be known as well. The uncertainties about the conditions prevailing at the dynamic wetting line make uncertain the reliability of the quantitative predictions of the flow field (Coyle et al., 1990). From experiments, Ghannam and Esmail (1997) showed that, for rotating rolls, the contact angle depends on the geometry of the wetted surface and the capillary number. Numerically, Hao and Haber (1999) found that the contact angle and the slip distance have a strong influence on the location of the three-phase line and the coating thickness. As a result, the numerical solution depends strongly on the conditions of the dynamic wetting line, and matching a set of experimental conditions to the numerical model requires specific values of the slip coefficient, slip length, and dynamic contact angle.

In numerical simulations, considering the cover deformation results in a better approximation of the coating flow hydrodynamics (Carvalho and Scriven, 1997; Fourcade et al., 1999). Consequently, parameters that are particularly sensitive to the nip elastohydrodynamic forces, such as the torque acting on the metering rod, become natural candidates for the assessment of the reliability of computational models. Torque measurements are at the basis of rotational rheometry (Macosko, 1994; Carreau et al., 1997), and they can also be adapted to mixing process rheometry (Brito et al., 1998). Although it is relatively simple to measure the torque on a rotating roll, only a few works have dealt with this issue (Alonso et al., 2000, 2001). From a fluid mechanics viewpoint, the torque signal may provide relevant information about the rheological conditions of the fluid in the metering nip, in the spirit of what has been obtained from experimental pressure measurements (Réglat and Tanguy, 1998; Alonso et al., 2000, 2001). Thus, the objective of this article is to use the torque signal on the rod and the nip pressure to assess the process viscosity models developed in film coating by means of computer fluid dynamic simulations of the metering nip flow. Newtonian fluids and paper coating colours are used under the typical conditions of the paper film coating process. Numerical simulations that consider the deformation of the roll cover as in Fourcade et al. (1999) are carried out. On the metering rod, both maximum pressure and torque are calculated and comparisons with experimental measurements are performed. In order to avoid the numerical complexity

associated with coupling an elastohydrodynamic model with a free surface algorithm, the nip is considered fully flooded. This simple two-dimensional model maintains the main features of the nip flow and is numerically more manageable than the entire representation of the free surface elastohydrodynamic reverse roll coating problem in three dimensions.

Physical and Numerical Experiments

The laboratory reverse roll coater used in the experiments is described in Alonso et al. (2000). Briefly, the metering rod is instrumented with a wall-mounted piezoelectric transducer to obtain the nip pressure profile at each revolution (Figure 1). A torque meter is directly connected to the shaft of the metering rod so that the torque signal is continuously monitored and recorded. Two displacement transducers, both located at each end of the rod, measure the relative position of the metering rod with respect to the undeformed surface of the transfer roll. The zero position is set when both rod and roll are in slight contact while being at rest.

Polyethylene glycol solutions at three concentrations (13.2%, 17% and 18.3% w/w) were used as Newtonian fluids. Three paper coating colour formulations were used, all based on 100 dry parts of clay, ten of latex, 0.04 of dispersant and with different CMC and solids contents as shown in Table 1.

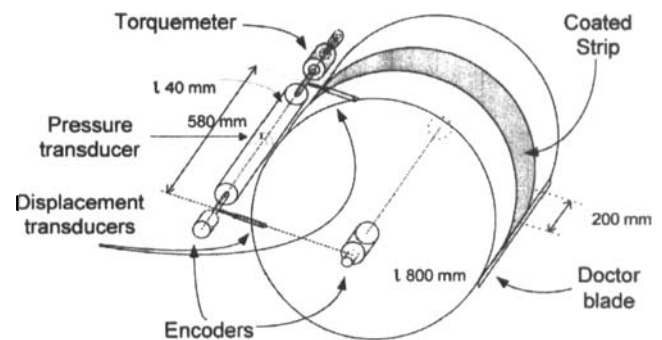


Figure 1. Instrumentation of the metering section of the laboratory coater.

Table 1. CMC and solids content in the coating colours.

Coating colour	CMC	% Solids
1	0.5	61.0
2	1.0	61.0
3	0.5	63.3

Table 2. Parameters of Cross model $\mu_{Cross} = \eta_{\infty} + [\eta_0 - \eta_{\infty}] / [1 + (t\dot{\gamma})^p]$.

Coating colour Label	t (s)	p	η_0 (Pa·s)	η_{∞} (Pa·s)	$ (\mu_{exp} - \mu_{Cross}) / \mu_{Cross} $
1	87	0.84	500	0.063	0.083
2	62.5	0.83	500	0.082	0.095
3	83	0.82	500	0.080	0.094

Table 3. Operating and geometrical parameters.

Variable	Nomenclature	Range
Transfer speed	V_t	500 – 1900 m/min
Metering rod speed	V_m	30 m/min
Experimental metering load	–	0.25–2.0 kN/m
Numerical nip gap	–	–40 – 80 mm
Transfer roll radius	R_t	0.40 m
Metering rod radius	R_m	0.02 m
Elastomer thickness	t_e	0.015 m
Metering nip length	l	0.02 m
Metered coated strip	–	0.2 m
Relaxation parameter	ω	0.3

The Cross model rheological parameters are showed in Table 2 (the details about their rheological characterization can be found in a related paper; Alonso et al., 2001). All the rheological parameters are similar and lie within the rheological behaviour of typical industrial paper coating colours. The low shear viscosity limit η_0 of the Cross model was chosen 500 Pa·s because it fits fairly well the rheological data obtained from the rheometer for each coating colour in the low shear region and eliminates computational problems. Choosing a higher value of η_0 for each coating colour would certainly improve the fitting since the coating colours do not have a low-shear viscosity plateau. Unfortunately, the higher the η_0 , the stiffer the solution of the numerical problem (higher viscosity gradients are generated) as pointed out in Roper and Attal (1993). In fact, the best fit would be a power law model with a high shear rate viscosity plateau (Iziquel et al., 1999), but, again, it would generate infinite viscosities at very low shear rates, making the numerical problem very difficult to solve (Roper and Attal, 1993).

The computational approach described in Fourcade et al. (1999) was used for the flow simulations. The computational domain, the nomenclature and the finite element elastohydrodynamic model are recalled in the Appendix (the simulation parameters are given in Table 3). The rigid-roll fluid problem is first solved. Next, the stress at the fluid–solid interface is used to calculate the force exerted by the fluid on the transfer roll. This force is then used to predict the cover deformation. Once the cover is deformed, the new fluid–solid interface generates new fluid and solid domains that are remeshed for the next iteration. The fluid problem is thus solved again, and this process is iterated upon until the normal force exerted by the fluid becomes equal to the elastic stresses. In practice, the fixed-point iteration procedure was applied until the fluid–solid normal stress residual value at the interface was equal or less than 3% of the fluid normal stress value [$(F_N - S_N)/F_N \leq 0.03$].

In the present study, the two-dimensional elastohydrodynamic problem was discretized with the Galerkin finite element method by means of the CFD code POLY2D™ (Rheotek Inc.) The meshing procedure was achieved using IDEAS™ (SDRC Inc.) Both fluid and solid meshes contained around 3400 and 4800 quadratic-interpolated triangular elements, respectively. Mesh refinement tests were performed to ensure that the results were independent of the mesh size. The remeshing procedure was such that the variation of the number of elements did not change appreciably so as to affect the

accuracy of the results from one iteration to the next one. Additionally, a relaxation parameter ω was used to avoid too large displacements and to ensure convergence.

The tangential force exerted by the fluid on the metering rod was used to calculate the torque T , namely:

$$T = R_m \int_{\Gamma_{fm}} (\sigma_F \cdot t_f) d\Gamma_{fm} \quad (1)$$

where R_m is the metering rod radius and Γ_{fm} the wetted surface of the rod to be integrated.

Results and Discussion

In this investigation, it is important to consider that, as explained in Réglat and Tanguy (1997), the experimental error in the calibration of the metering rod relative position can be up to 20 mm, a value that may be kept in mind when analyzing the results. The size of the pressure transducer may be another source of systematic error. It is relatively large (2.5 mm in diameter) with respect to the total length of the nip (~13 mm) so that the experimental pressure is an average value on the surface of the transducer. This effect was somehow considered in the numerical results by averaging the pressure profile in a distance of 2.5 mm, yet the error associated with this approximation may be added to the discrepancy between the numerical results and the experimental data (Réglat and Tanguy, 1997). Finally, the fluids used in this investigation contained a significant solids content, but the numerical model considers only one single phase and consequently neglects particle interactions. Assuming minimal sources of error, the numerical simulations were used to assess the methods of evaluation of the process viscosity models of Alonso et al. (2000, 2001).

Process Viscosity Maximum Pressure

The process viscosity is defined as the shear viscosity of a Newtonian fluid that would yield the maximum pressure of a non-Newtonian fluid at the same flow conditions (Réglat and Tanguy, 1998). In the method, the maximum pressure is first measured with Newtonian fluids at different V_t 's, nip gaps, and viscosities so that $P_{max} = P_{max}(V_t, \text{nip gap}, \mu_{ss})$ (Réglat and Tanguy, 1997). This equation is differentiated to approximate the dependency of the maximum pressure on the process variables. At the end, for coating colours, the maximum pressure is measured and used in the differential equation to estimate the viscosity of the coating colours following the definition of the process viscosity μ_{proc}^P . With this procedure (Alonso et al., 2000), the calculated process viscosity μ_{proc}^P of the coating colours was found to be significantly higher than the steady state shear viscosity μ_{ss} obtained in a rheometer (Table 4).

Figure 2a displays the variation of the maximum pressure values with respect to the metering rod position for two coating colours. From the fact that the experimental curve is below the numerical results, one can infer that the parameters for the steady state shear viscosity predicted by the Cross model overestimate the viscosity of the coating colours. The use of the process viscosity μ_{proc}^P in the numerical simulations would result in an even higher difference between the numerical and experimental results since μ_{proc}^P is about six times higher than the Cross model viscosity (a more viscous fluid generates a higher maximum pressure). This behaviour is of course surprising since

Table 4. Process, transient, steady state and plateau viscosities for the coating colours.

Viscosity (Pa·s)	μ_{proc}^P	μ_{proc}^T	μ_{proc}	η^+	μ_{ss} at 1000 s ⁻¹	η_{∞} (Cross)
Colour	Alonso et al. (2000a)		Alonso et al. (2000b)			
1	0.478	0.063	0.019	0.082	0.095	0.063
2	0.645	0.069	0.022	0.140	0.129	0.082
3	0.641	0.062	0.070	0.103	0.108	0.080

one would expect that using the process viscosity in the numerical model yielded more accurate results, i.e., to decrease the difference between the numerical and experimental data by decreasing the numerical maximum pressure.

The discrepancies may be linked to the location of the maximum pressure and the rheological behaviour of the coating colours under extensional flow. Between rolls, the maximum pressure is located upstream from the nip centre (Gaskell et al., 1998), i.e., in the converging region of the nip, where shear and extensional flows coexist. The fact that a converging-diverging channel can be used to investigate the extensional behaviour of the coating colours through pressure measurements (Isaksson et al., 1998; Lavoie et al., 1997) suggests that the extensional behaviour of the coating colours greatly influences the values of the process viscosity μ_{proc}^P . This effect can be explained by the occurrence that, for a set of operating conditions of transfer speed and rod position, the maximum pressure depends on the extensional α_e and shear α_s flow contributions (Réglat and Tanguy, 1998) as:

$$\frac{\Delta P_{max}}{\Delta \mu_{ss}} = \alpha_s + k\alpha_e \quad (2)$$

where $\alpha_s = \partial P_{max} / \partial \mu_{ss}$ and $\alpha_e = \partial P_{max} / \partial \mu_e$ and k is the Trouton ratio, i.e., the ratio of extensional to shear viscosity. For Newtonian fluids, there is no stretching, $\alpha_e = 0$, and the term $\partial P_{max} / \partial \mu_{ss}$ (or $\Delta P_{max} / \Delta \mu_{ss}$) can be evaluated directly from experiments (Réglat and Tanguy, 1998; Alonso et al., 2000). For non-Newtonian

fluids, α_s is still valid but k and α_e may be a function of the extension rate. k can be known from experiments in an extensional rheometer, but α_e can only be evaluated explicitly from tests in the film coater with fluids with different extensional viscosities and constant shear viscosity. As a result, the coating colour process viscosity μ_{proc}^P evaluated from maximum pressure measurements may change — depending on the values of α_e and k — when the extensional behaviour of the fluids is taken into account.

Torque

The process viscosity μ_{proc}^T represents a value of the fluid viscosity based upon the global shear and extensional conditions that prevail within the metering nip. This procedure requires a dimensional analysis of the metering nip, the measure of the torque for Newtonian fluids (used as reference) and coating colours and applies the concept of Metzner and Otto (1957) used in the theory of mixing. To evaluate μ_{proc}^T , the process shear rate was estimated as $\dot{\gamma}_{proc} = K_s V_t / H$. K_s is the constant of Metzner and Otto for the torque behaviour in the nip that depends on both Newtonian fluids (K_p) and coating colours ($K_{p,n}$), the latter considered as power law fluids. In the reference (Alonso et al., 2000), the process viscosity μ_{proc}^T was found lower than the viscosity μ_{ss} obtained in the rheometer (Table 4).

Figure 2b shows the variation of the experimental and numerical torque values with respect to the metering rod relative position. One may readily observe that the discrepancies are more significant than in the case of the maximum pressure measurements. One can also infer from these results that the

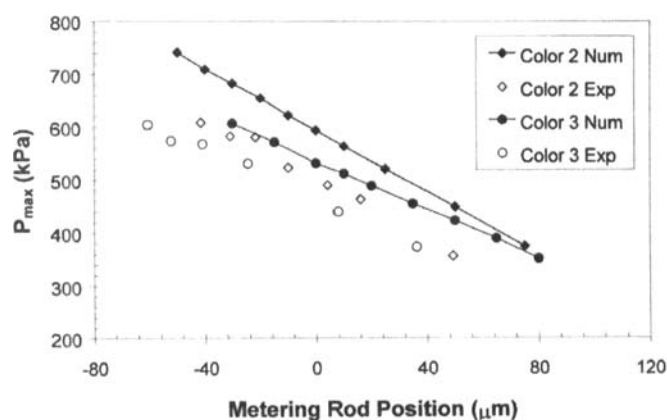


Figure 2a. Variation of the maximum pressure with the metering rod position for two different coating colours ($V_t = 1750$ m/min, $V_m = 30$ m/min).

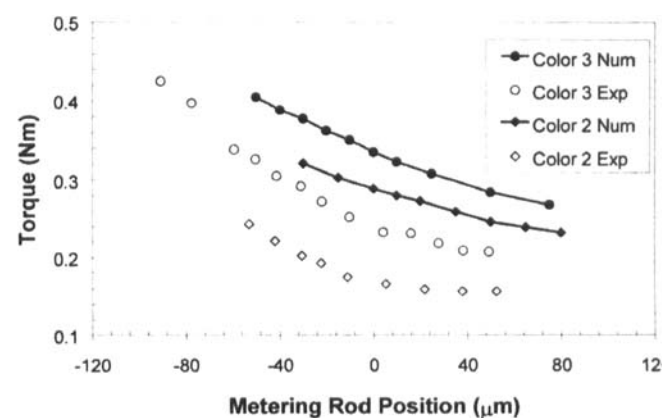


Figure 2b. Variation of the torque with the metering rod position for two different coating colours ($V_t = 1750$ m/min, $V_m = 30$ m/min).

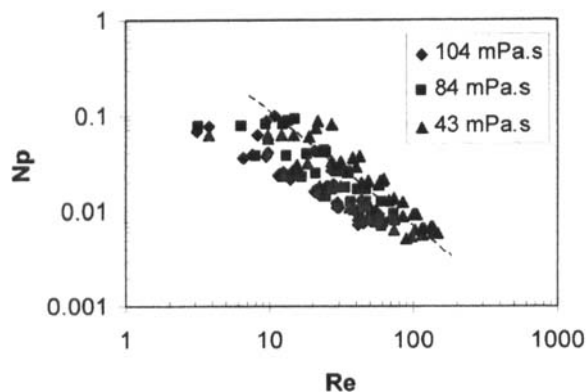


Figure 3a. Power number as function of the Reynolds number for Newtonian fluids.

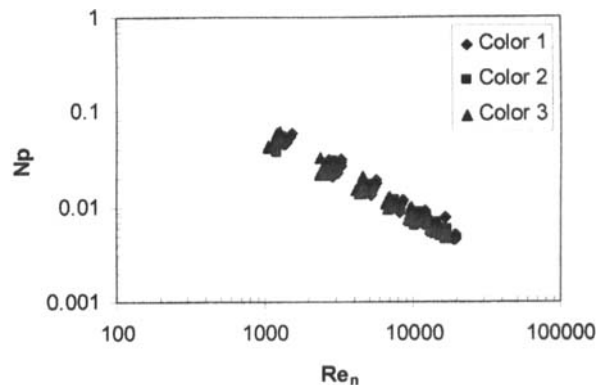


Figure 3c. Power number as function of the Reynolds number for coating colours.

rheological parameters of the Cross model overestimate the viscosity in all cases since the experimental results are below the numerical curve. From a rheological standpoint, two comments are in order. In mixing, the Metzner and Otto concept (Metzner and Otto, 1957) was developed for laminar flow. Since Alonso et al. (2000) does not mention the regime underlying their process viscosity evaluations, their results are revisited in this work. In order to better account for the physics of the problem (regarding the analogy with a mixing system), a new dimensional analysis is carried out. The power number is redefined as $Np = C_{proc}/SV_t^2 R_m \rho$, the Reynolds number is $Re = \rho V_t H / \mu_{ss}$, and $Kp = Np \cdot Re$ for Newtonian fluids, and $Re_n = \rho V_t^{2-n} H_n / m (V_t/H)^{n-1}$, and $Kp_n = Np \cdot Re_n$ for the coating colours, both Kp and Kp_n are constants in the laminar regime (Sterbáček and Tausk, 1965); finally, C_{proc} is the effective torque measured on the wetted area S of the metering rod, V_t is the transfer speed, R_m the rod radius, ρ the density, H the calculated nip gap, and m and n the power law parameters. We give in Figure 3 the Np and Kp curves obtained for Newtonian fluids and coating colours. It comes from experiments and dimensional analysis that the slope of an Np vs. Re curve should be equal to -1 (logarithmic scale) in the laminar regime and decrease to near zero in the fully turbulent regime (Sterbáček and Tausk, 1965). The slope of -1 is

independent of the index n of the power law rheological model so that the Metzner and Otto concept works for both shear-thinning and shear-thickening fluids (Tanguy et al., 1996), common rheological behaviours observed in coating colours (Laun and Hirsch, 1989; Roper and Attal, 1993).

Figure 3a shows the variation of Kp with respect to the Reynolds number. Each data series (represented by the dotted line) corresponds to a constant load but different transfer speeds and nip gaps. The geometric constant Kp (Figure 3b) appears to be a function of the Reynolds number for Newtonian fluids. These variations are mostly owing to the fact that different gaps correspond to different nip geometries and hence, in the spirit of dimensional analysis, to different processes. Figure 3c shows the $Np-Re_n$ curves for the coating colours, results that depict a behaviour similar to that of the Newtonian fluids. Kp curves (Figure 3b and 3d) reveal that the Kp values range from 0.2 to 2.15 in the Newtonian case and from 45 to 125 for the coating colours. Such Kp and Kp_n variations make it difficult to use the concept of Metzner and Otto. As a result, the concept of process viscosity should be applied at low speed, in order to ensure the laminar regime and minimize the influence of the nip gap on the geometric constant Kp .

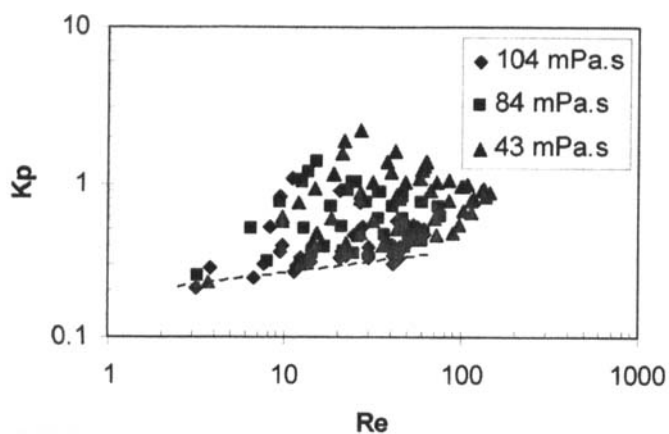


Figure 3b. Kp as function of the Reynolds number for Newtonian fluids.

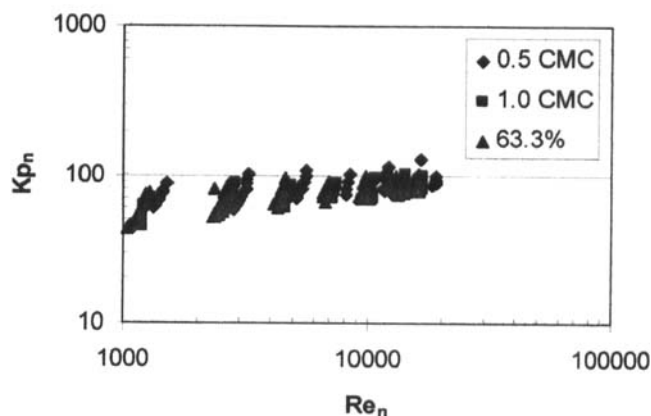


Figure 3d. Kp_n as function of the Reynolds number for coating colours.

The torque-based methodology presented above considers that the coating colours are power law fluids. Consequently, the very high Reynolds numbers calculated for the coating colours (Figs. 3c and 3d) are a consequence of the very small viscosity predicted by the power law model at the shear rates of the coating process ($\sim 10^5 \text{ s}^{-1}$). In the metering nip, however, the rheological model is likely to perform poorly because the shear rates are such that the viscosity may be on the Newtonian plateau (Alonso et al., 2001). In order for the coating colours to behave as power law fluids, the shear rates and speeds should be low, which were not the work conditions of Alonso et al. (2000). As a result of both remarks, the torque-based procedure for evaluating the process viscosity is suitable only when the shear rates and process speeds are small.

Pressure and Torque Combined

The two methods proposed above suffer from drawbacks that come from the speed and converging-diverging geometry of the metering nip. Thus, by considering a region within the nip where the flow is shear-dominated — the nip centre, for example — the uncertainty with respect to the extensional effects on the flow can be considerably reduced. Additionally, the transient nature of the metering nip flow (Laun and Hirsch, 1989; Cohu and Magnin, 1995) brings the idea that the process viscosity should be compared with transient rheological tests in the rheometer. Both of these issues were considered in the methodology proposed in a previous paper (Alonso et al., 2001). This methodology combines the pressure gradient and the torque by means of the *lubrication theory* applied in the centre of the nip and requires no Newtonian reference fluids. With this method (Alonso et al., 2001), the values of the process viscosity μ_{proc} , the viscosity of the coating colour in the centre of the nip, were found to be lower than the transient viscosity η^+ obtained with step growth tests in a rheometer (see the values in Table 4).

A few comments must be made about the coating colour rheology. In Table 4, the values of the transient viscosity η^+ (obtained 0.1 s after a step growth test from 80 s^{-1} to 1000 s^{-1} in Alonso et al., 2001) are very close to the steady state viscosity values μ_{ss} but higher than the viscosity plateau η_∞ estimated from fitting the rheological data to the Cross model. Thus, one would expect that using the values of η^+ in the numerical simulations give a larger difference between the numerical and experimental results than those obtained from the Cross model. The only suitable viscosity that allows to decrease the numerical results is then the process viscosity μ_{proc} (the process viscosity from the torque methodology μ_{proc}^T could also shift down the numerical curve but it does not perform properly).

An additional issue of importance is the use of the torque measurements in the evaluation of the process viscosity μ_{proc} . From the numerical simulations (Alonso et al., 2001), it is observed that the stress values change with the position, with positive and negative values. This change in sign may make it difficult to use the torque in the evaluation of the process viscosity in the whole nip. The process viscosity μ_{proc} was evaluated exclusively in the centre of the nip (with a pressure gradient almost constant), where the shear stress is always positive, although not constant. The methodology considers the integral of the stress in that region only; thus, the process viscosity μ_{proc} regarding the torque measurements is an average value represented by the area under the stress curve in the region of almost constant pressure gradient. Since experimentally it is not

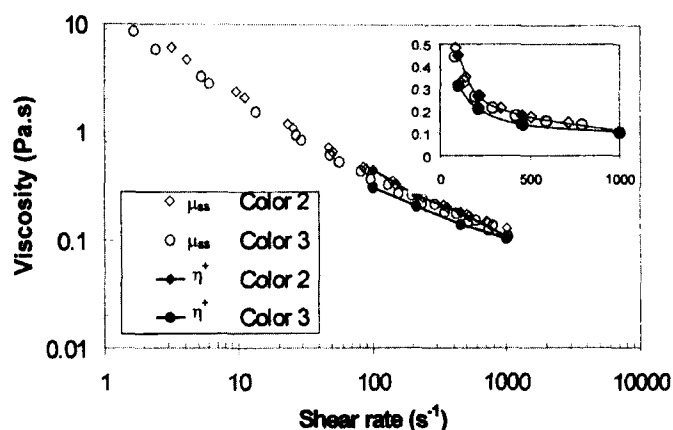


Figure 4. Steady rate and transient viscosities for two coating colours.

possible to measure the torque in such region, a numerical procedure was adapted to deduce the experimental torque that corresponds to the region of application of the lubrication theory (Alonso et al., 2001). That is also the region of maximum shearing, i.e., the minimum viscosity the fluid can have when passing through the nip. As a result, this process viscosity μ_{proc} is the one that the coating colour has in the metering nip and before arriving to the application nip (Alonso et al., 2001).

The time and shear dependence of the coating colours does not allow us to use directly in the simulations the process viscosity μ_{proc} . We illustrate this in Figure 4, which shows the steady state shear viscosity μ_{ss} for two coating colours. The other η^+ curves were constructed from the rheological results obtained after an initial preshearing of the sample at 80 s^{-1} for 30 s and then applying step growth tests up to 1000 s^{-1} (the readings were taken 0.1 s after the increase in shear rate). The values of this transient viscosity η^+ decrease with the step growth rate level and follow also the trend of the steady state viscosity. The transient values are slightly below, but the differences can be better seen by zooming the high shear region (these differences in viscosity are enough to change the hydrodynamics of the metering nip flow, i.e., the pressure profile; Réglat and Tanguy, 1997, 1998; Alonso and Tanguy, 2001). This transient viscosity η^+ behaviour for coating colour 3 could be fitted with the Cross model with the following parameters: $p = 0.79$ and $t = 150 \text{ s}$.

New numerical experiments were performed with the transient Cross model parameters in order to consider somehow the shear and time dependence of the fluid upstream the metering nip. In the centre, we believe that the viscosity of the coating colour is that approximated from the combination of the pressure gradient and torque methodology, μ_{proc} by means of the lubrication theory. Thus, this process viscosity μ_{proc} of colour 3 was used as viscosity plateau in what we called a semi-analytical rheological model. The results are shown in Figure 5, in which one can observe that the use of this rheological model shifts down the numerical curve and brings it closer to the experimental results. The remaining smaller difference then suggests that this model needs further improvements.

From the discussion of above, a very important question arises: what rheological model should be used in the simulations of the metering nip flow? Since the colour has no time to

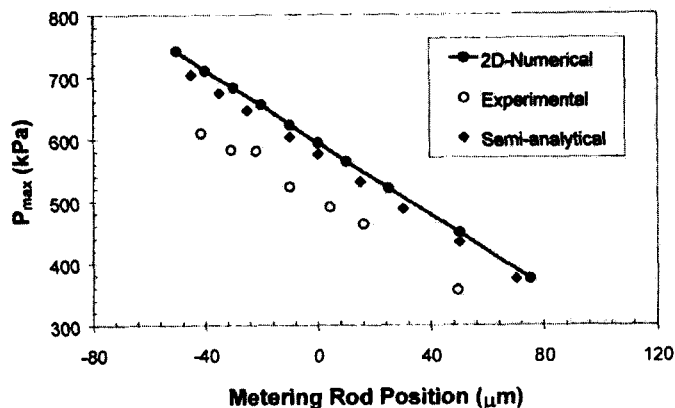


Figure 5. Maximum pressure vs. metering rod relative position for colour 3 ($V_t = 1750$ m/mn, $V_m = 30$ m/min).

restructure before arriving to the application nip (Alonso et al., 2001), a suitable assumption may be to consider that the coating colour behaves as Newtonian downstream the nip, with a viscosity equal to the process viscosity μ_{proc} . Upstream the nip, the fact that the mixing procedure used in the coating colour makedown may affect the coating colour rheological behaviour and runnability (Persson et al., 1997; Alonso and Tanguy, 2001) suggests that the shear preconditioning may affect the measurements in the film coater, plus the possible effect of the extensional behaviour of the coating colours. Thus, more rheological tests are needed in order to clarify the relative influence of time, preconditioning and the extensional behaviour of the coating colours.

For the time being, the combination of transient rheological tests with the process viscosity in a semi-analytical model is a clear improvement of the metering nip flow although it certainly admits further enhancements. For example, improvements in the transient rheological tests may be made by using a more powerful rheometer (in this investigation the lowest reliable time to perform the step growth tests was 2 s with a data acquisition response time estimated in 0.1 s, far long compared to the residence time of milliseconds in the metering nip). We must also keep in mind that each coating formulation has its own rheological behaviour so that what was observed in this work may be different with other formulations. A further analysis with more complex coating industrial coating colours is needed, including some fluids with a rheological behaviour different than that of the fluid presented here, and licensed industrial formulations. Finally, the process viscosity may also be related to the occurrence of instabilities in the metering and application nips, which will be the topic of future work.

Conclusion

In a laboratory film coater, the hydrodynamic pressure and the torque signal on the metering rod were used to investigate the coating colour rheological behaviour in the metering nip. Numerical simulations were used as a key to assess the process viscosity of the coating colours from former publications. From the valuable points arrived at in this work, it was found that the maximum pressure may be preferably used to evaluate the process viscosity when the extensional behaviour of the coating

colours is known. The torque may be used to determine the process viscosity when the coating colours are subjected to low shear rates and follow the power law rheological model. Our major contribution here is the finding that the process viscosity evaluated in a region of shear-dominated flow is the one that can better describe the hydrodynamics of the metering nip flow. This was found by making a combination of the process viscosity with an adapted transient Cross model, idea proposed as a first attempt at exploring the numerical description of the coating colours rheological behaviour in the nip since it better approximates the flow hydrodynamics than the steady state rheological model alone.

Appendix

The computational domain for the simulations is shown in Figures A1 and A2. V_m and V_t are the speeds of the metering rod and the transfer roll, respectively, l is the length of the domain, H defines the minimum clearance between rod and roll before deformation, and t_e is the thickness of the elastic cover. Ω_f is the computational domain for the fluid and Ω_s that for the solid, Γ_f is the fluid boundary, Γ_s the solid boundary, and Γ the solid-fluid interface along the transfer roll. Γ_{ft} is the fluid boundary along the transfer roll surface, Γ_{fm} the fluid boundary along the metering rod surface, Γ_{st} the solid boundary along the transfer roll, \mathbf{n}_f the unit vector normal to Γ_{ft} , \mathbf{n}_s the unit vector normal to Γ_{st} and \mathbf{t}_f the unit vector tangent to Γ_{fm} .

Fluid Problem

The flow of an incompressible fluid in the computational fluid domain Ω_f with boundary Γ_f is governed by the 2-D momentum and continuity equations:

$$\begin{aligned} \text{div } \sigma_F - \rho \mathbf{v} \cdot \text{grad } \mathbf{v} &= 0 & \text{in } \Omega_f \\ \text{div } \mathbf{v} &= 0 & \text{in } \Omega_f \end{aligned} \quad (\text{A1})$$

where the total stress and the rate-of-strain tensors are defined as:

$$\sigma_F = -p\delta + 2\mu\dot{\gamma} \quad (\text{A3})$$

$$\dot{\gamma} = \frac{1}{2} [\text{grad } \mathbf{v} + (\text{grad } \mathbf{v})^T] \quad (\text{A4})$$

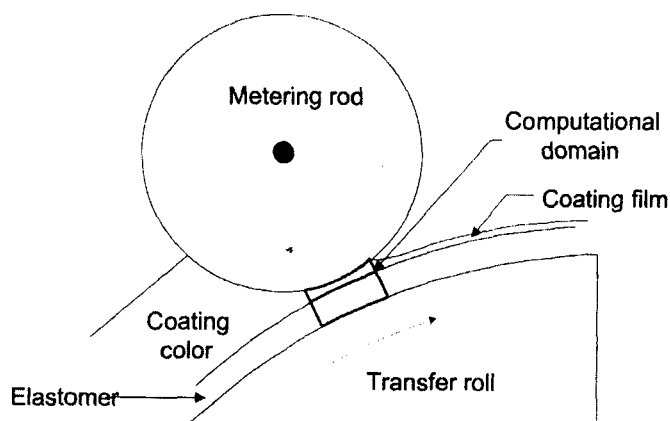


Figure A1. Computational domain in the simulation of the metering nip.

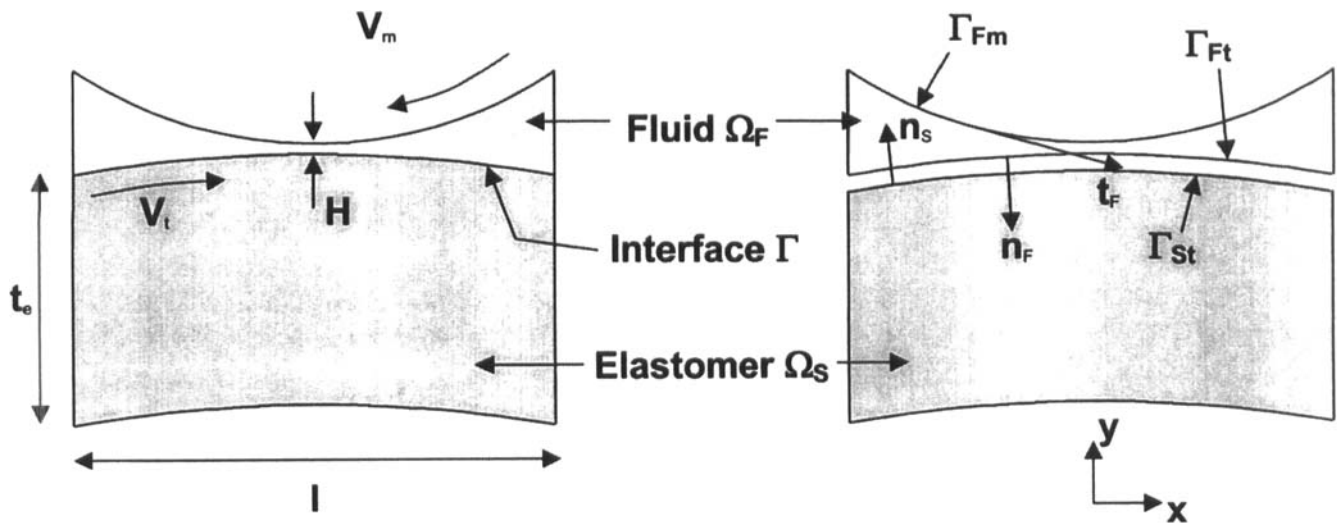


Figure A2. Nomenclature of the computational domain.

In this paper, rheological behaviour of the coating colours was approximated with the Cross model due to its improved numerical stability (Roper and Attal, 1993):

$$\mu_{\text{Cross}} = \eta_{\infty} + \frac{\eta_0 - \eta_{\infty}}{1 + (\dot{\gamma})^p} \quad (\text{A5})$$

The following essential boundary conditions are imposed:

$$\mathbf{v} = V_t \quad \text{on } \Gamma_{Ft} \quad (\text{A6})$$

$$\mathbf{v} = V_m \quad \text{on } \Gamma_{Fm} \quad (\text{A7})$$

together with the natural boundary conditions:

$$(\sigma_F)_{nn} = 0 \quad \text{on } \Gamma_F \setminus (\Gamma_{Ft} \cup \Gamma_{Fm}) \quad (\text{A8})$$

$$(\sigma_F)_{nt} = 0 \quad \text{on } \Gamma_F \setminus (\Gamma_{Ft} \cup \Gamma_{Fm}) \quad (\text{A9})$$

where \mathbf{n} stands for the outward unit vector normal to Γ_F (Γ_{Ft} , Γ_{Fm}), the extremities of the nip.

On the metering rod, the total torque exerted on the rod is calculated as:

$$T = R_m \int_{\Gamma} (\sigma_F \cdot \mathbf{t}_F) d\Gamma \quad \text{on } \Gamma \quad (\text{A10})$$

Solid Problem

The evaluation of the displacement \mathbf{u} of the elastomer cover under the influence of hydrodynamic forces is carried out under the following assumptions:

- The displacements \mathbf{u} are small.
- The elastomer is isotropic and homogeneous.
- The elastomer elasticity obeys Hook's law.
- The elastomer is incompressible.

The linearized strain tensor is:

$$\epsilon = \frac{1}{2} [\text{grad } \mathbf{u} + (\text{grad } \mathbf{u})^T] \quad (\text{A11})$$

and the displacements \mathbf{u} of the elastomer cover are governed by the two-dimensional Stokes-like equations:

$$\text{div } \sigma_s = 0 \quad \text{in } \Omega_s \quad (\text{A12})$$

$$\text{div } \mathbf{u} = 0 \quad \text{in } \Omega_s \quad (\text{A13})$$

$$\text{with} \quad (\text{A14})$$

$$\sigma_s = 2G\epsilon + q\delta$$

where G is the shear modulus and can be related to the Young's modulus E as $G = E/3$, and where q is a Lagrange multiplier introduced to enforce the incompressibility constraint.

The cover of the transfer roll deforms only when it is in contact with the fluid. As a consequence, the following Dirichlet boundary condition is set:

$$\mathbf{u} = 0 \quad \text{on } \Gamma_s \setminus \Gamma_{st} \quad (\text{A15})$$

At equilibrium, the stress balance between the hydrodynamic and elastic stresses satisfies:

$$\sigma_F \cdot \mathbf{n}_F + \sigma_S \cdot \mathbf{n}_S = (\sigma_S - \sigma_F) \cdot \mathbf{n}_S = 0 \quad \text{on } \Gamma \quad (\text{A16})$$

which is in fact a Neumann boundary condition that provides the load for the elasticity problem (A12) to (A13).

The stresses that build up in the elastomer are stored so that they can be used in the following iteration. A continuation method can also be used when one-go simulations are difficult to carry out. A given set of parameters for which the solution is known can be used to generate a new solution for a different

set of parameters where one or several variables can be modified. For example, this method has helped achieve convergence when negative gaps have been required (Fourcade et al., 1999).

Acknowledgments

The financial contributions of Paprican, NSERC (Canada), and Conacyt (Mexico) are gratefully acknowledged.

Nomenclature

C_{proc}	effective torque measured on the metering rod, (N·m)
F_N	fluid normal stress, (Pa)
H	calculated nip gap, (m)
k	Trouton ratio
K_s	Metzner and Otto constant in the evaluation of the process shear rate
m	consistency index in the power law model, (Pa·s ^{<i>n</i>})
n	power index in the power law model
p	shear-thinning index in the Cross model
P_{max}	maximum pressure within the metering nip, (Pa)
R_t	transfer roll radius, (m)
R_m	metering rod radius, (m)
S	wetted surface on the metering rod, (m ²)
S_N	solid normal stress, (Pa)
t	consistency index in the Cross model, (s)
t_F	tangent vector for the fluid domain
T	calculated torque on the metering rod, (N·m)
V_t	transfer roll speed, (m/s)

Greek Symbols

α_e	extensional flow contribution to the maximum pressure, (1/s)
α_s	shear flow contribution to the maximum pressure, (1/s)
$\dot{\gamma}$	shear rate, (1/s)
$\dot{\gamma}_{proc}$	process shear rate, (1/s)
Γ_{fm}	solid–fluid interface along the metering rod
η^+	transient viscosity, (Pa·s)
η_0	viscosity plateau at low shear rates, (Cross model) (Pa·s)
η_∞	viscosity plateau at high shear rates, (Cross model) (Pa·s)
μ_{Cross}	cross model viscosity, (Pa·s)
μ_{ss}	steady state shear viscosity, (Pa·s)
μ_e	extensional viscosity, (Pa·s)
μ_{proc}^P	process viscosity calculated from pressure measurements, (Pa·s)
μ_{proc}^T	process viscosity calculated from torque measurements, (Pa·s)
μ_{proc}	process viscosity from the lubrication approximation, (Pa·s)
σ_F	stress tensor for the fluid
	density, (kg/m ³)
ω	relaxation parameter

References

Alonso, S. and P.A. Tanguy, "Hydrodynamic Instabilities in the Metering Nip of a Film Coater", *Tappi J.* **84** (2001).

Alonso, S., O. Réglat, F. Bertrand and P.A. Tanguy, "Process Viscosity in a Film Coater", *Paperi ja Puu (Paper and Timber)* **82**, 34–40 (2000).

Alonso, S., O. Réglat, F. Bertrand, L. Choplin and P.A. Tanguy, "Process Viscosity in Reverse Roll Coating", *Chem. Eng. Res. & Des.* **70**, 128–136 (2001).

Brito-de la Fuente, E., J.A. Nava, L.M. Lopez, L. Medina, G. Ascanio and P.A. Tanguy, "Process Viscosimetry of Complex Fluids and Suspensions with Helical Ribbon Agitators", *Can. J. Chem. Eng.* **76**, 689–695 (1998).

Carreau, P.J., D. De Kee and R.P. Chhabra, "Polymer Rheology: Principles and Applications", Hanser, Munich, Germany (1997).

Carvalho, M.S. and L.E. Scriven, "Effect of Deformable Roll Cover on Roll Coating", in "Proc. Tappi Pol. Lam. and Coat. Conf.", Tappi, Atlanta, GA (1993), pp.451–459.

Carvalho, M.S. and L.E. Scriven, "Deformable Roll Coating Flows: Steady State and Linear Perturbation Analysis", *J. Fluids Mech.* **339**, 143–172 (1997).

Carvalho, M.S. and L.E. Scriven, "Three-Dimensional Stability Analysis of Free Surface Flows: Application to Forward Deformable Roll Coating", *J. of Comp. Phys.* **151**, 534–562 (1999).

Cohu, O. and A. Magnin, "Rheometry of Paints with Regard to Roll Coating Process", *J. Rheol.* **39**, 767–785 (1995).

Coyle, D. "Forward Roll Coating with Deformable Rolls: A Simple One-Dimensional Elastohydrodynamic Model", *Chem. Eng. Sci.* **43**, 2673–2684 (1988).

Coyle, D., C.W. Macosko and L.E. Scriven, "The Fluids Dynamics of Reverse Roll Coating", *AIChE J.* **36**, 161–174 (1990).

Fourcade, E., F. Bertrand, O. Réglat and P.A. Tanguy, "Finite Element Analysis of Fluid–Solid Interaction in the Metering Nip of a Metering Size Press", *Comp. Meth. In Appl. Mech. and Eng.* **174**, 235–245 (1999).

Gaskell, P.H., G.E. Innes and M.D. Savage, "An Experimental Investigation of Meniscus Roll Coating", *J. Fluid Mech.* **355**, 17–44 (1998).

Ghannam, M.T. and N.B. Esmail, "Effect of Substrate Geometry on Dynamic Contact Angles in Surface Wetting", *Chem. Eng. Comm.* **159**, 43–57 (1997).

Hao, Y. and S. Haber, "Reverse Roll Coating Flow", *Int. J. Num. Meth. in Fluids* **30**, 635–652 (1999).

Isaksson, P., M. Rigdahl, P. Flink and S. Forsberg, "Aspects of the Elongational Flow Behavior of Coating Colors", *J. Pulp and Paper Sci.* **24**, 204–209 (1998).

Iziquel, F., P.J. Carreau, M. Moan and P.A. Tanguy, "Rheological Modelling of Concentrated Colloidal Suspensions", *J. Non-Newt. Fl. Mech.* **86**, 133–155 (1999).

Laun, H.M. and G.X. Hirsch, "New Laboratory Tests to Measure Rheological Properties of Paper Coatings in Transient and Steady-State Flows", *Rheol. Acta* **28**, 267–280 (1989).

Lavoie, P.A., P.J. Carreau and T. Ghosh, "Rheology of Suspensions: The Flow Behavior of Coating Colors", *J. Pulp Paper Sci.* **23**, 543–547 (1997).

Macosko, C.W., "Rheology, Principles, Measurements and Applications", VCH Publishers, USA (1994).

Metzner, A.B. and R.E. Otto, "Agitation of Non-Newtonian Fluids", *AIChE J.* **3**, 3–10 (1957).

Persson, T., L. Järnström and M. Rigdahl, "Effect of Method of Preparation of Coating Colors on the Rheological Behavior and Properties of Coating Layers and Coater Papers", *Tappi J.* **80**, 117–124 (1997).

Réglat, O. and P.A. Tanguy, "An Experimental Study of the Flow in the Metering Nip of a Metering Size Press", *AIChE J.* **80**, 2911–2920 (1997).

Réglat O. and P.A. Tanguy, "Rheological Investigations of CaCO₃ Slurries in the Metering Nip of a Metering Size Press", *Tappi J.* **81**, 195–205 (1998).

Roper, D.A. and J.F. Attal, "Evaluations of Coating High-Speed Runnability Using Pilot Plant Coater Data, Rheological Measurements and Computer Modeling", *Tappi J.* **76**, 55–62 (1993).

Sterbáček, Z. and P. Tausk, "Mixing in the Chemical Industry", Pergamon press, 78–81 (1965).

Tanguy, P.A., F. Thibault and E. Brito de la Fuente, "A New Investigation of the Metzner-Otto Concept for Anchor Mixing Impellers", *Can. J. Chem. Eng.* **74**, 222–228 (1996).

Wickström, M. and J. Grön, "Formation of Patterns on Paper Coated with Metering Size Press", *Proc. Tappi Coat. Conf. and Trade Fair. Tappi, Atlanta, GA (2000)*, pp. 355–366.

Manuscript received August 23, 2000; revised manuscript received March 20, 2001; accepted for publication May 28, 2001.